MIT Open Access Articles

Regional Climate Modeling over the Maritime Continent. Part I: New Parameterization for Convective Cloud Fraction

Massachusetts Institute of Technology

Regional Climate Modeling over the Maritime Continent. Part I: New Parameterization for Convective Cloud Fraction

REBECCA L. GIANOTTI AND ELFATIH A. B. ELTAHIR

Ralph M. Parsons Laboratory, Massachusetts Institute of Technology, Cambridge, Massachusetts

(Manuscript received 21 February 2013, in final form 6 August 2013)

ABSTRACT

This paper describes a new method for parameterizing convective cloud fraction that can be used within large-scale climate models, and evaluates the new method using the Regional Climate Model, version 3 (RegCM3), coupled to the land surface scheme Integrated Biosphere Simulator (IBIS). The horizontal extent of convective cloud cover is calculated by utilizing a relationship between the simulated amount of convective cloud water and typical observations of convective cloud water density. This formulation not only provides a physically meaningful basis for the simulation of convective cloud cover, but it is also spatially and temporally variable and independent of model resolution, rendering it generally applicable for large-scale climate models. Simulations over the Maritime Continent show that the new method allows for simulation of an essential convective–radiative feedback, which was absent in the existing version of RegCM3–IBIS, such that moist convection not only responds to diurnal variability at the earth's surface but also impacts the solar radiation received at the surface via cumulus cloud production. The impact on model performance was mixed, but it is considered that appropriate representation of the convective–radiative feedback and improved physical realism resulting from the new cloud fraction parameterization will likely have positive benefits elsewhere. The role of convective rainfall production in the convective–radiative feedback and a new parameterization for convective autoconversion are addressed in Part II of this paper series.

1. Introduction

While the skill of large-scale climate models in reproducing the existing climate has improved significantly over many parts of the world, simulations over the Maritime Continent region still contain substantial error (e.g., Yang and Slingo 2001; Neale and Slingo 2003; Dai and Trenberth 2004; Wang et al. 2007). This error propagates into future rainfall projections that vary so widely between models as to disagree on the sign of the change (Christensen et al. 2007).

Gianotti et al. (2012) showed that the Regional Climate Model, version 3.0 (RegCM3), coupled with the land surface scheme Integrated Biosphere Simulator (IBIS) exhibited significant error over the Maritime Continent region with respect to rainfall, net radiation, latent and sensible heat fluxes, and evapotranspiration over the land surface. The authors noted that these errors were not unique but instead were consistent with

other published climate modeling studies conducted over the Maritime Continent region (e.g., Chow et al. 2006; Francisco et al. 2006; Martin et al. 2006; Wang et al. 2007). It was argued that the source of the errors resided primarily in the atmospheric component (i.e., RegCM3) of the coupled model system, specifically with the simulation of convective rainfall (Gianotti et al. 2012).

Convection is initiated primarily within the planetary boundary layer (PBL) region, which responds on relatively short time scales to surface turbulent heat fluxes driven by incoming radiation. Convective activity influences large-scale atmospheric dynamics not only through diabatic heating and vertical transports of heat and moisture, but also through the interaction of cumulus clouds with radiation (Tiedtke 1988). The strong interaction of cumulus clouds with both shortwave and longwave radiation alters the distribution of surface and atmospheric heating. In turn, this drives the atmospheric motion that is responsible for cloud formation, including the variability associated with atmospheric convection (Bergman and Salby 1996), thus creating a convective–radiative feedback.

Corresponding author address: Rebecca L. Gianotti, MIT Room 48-207, 15 Vassar Street, Cambridge, MA 02139.
E-mail: rlg@alum.mit.edu

Despite significant improvements over recent decades in the ability of large-scale climate models to reproduce the existing climate and its sensitivity, the representation of clouds and cloud-related processes remains extremely problematic. Cloud feedbacks were identified as a primary reason for differences between models in the Intergovernmental Panel on Climate Change Fourth Assessment Report (IPCC AR4), with the shortwave impact of boundary layer and midlevel clouds making the largest contribution (Christensen et al. 2007). However, few studies have been undertaken to evaluate the performance of large-scale climate models with respect to cloud cover and radiative fluxes over the tropics.

Kothe and Ahrens (2010) evaluated the monthly radiation budget over West Africa as simulated by eight different regional climate models (RCMs), which contributed to the European Union Ensemble-Based Predictions of Climate Changes and Their Impacts (ENSEMBLES) project. It was shown that most of the models generally underestimated surface net shortwave radiation in ocean areas and in parts of the intertropical convergence zone (ITCZ). It was also shown that most models overestimated cloud fraction, especially over ocean and in the equatorial region, which accounted for more than 20% of the radiative flux errors over land and more than 40% over ocean (Kothe and Ahrens 2010).

Lin and Zhang (2004) evaluated cloud climatology and the cloud radiative forcing at the top of the atmosphere as simulated by the National Center for Atmospheric Research (NCAR) Community Atmospheric Model, version 2 (CAM2). It was shown that the model overestimated total cloud amount in the western Pacific Ocean, Maritime Continent, and central Africa but simulated reasonable cloud radiative forcing at the top of the atmosphere (Lin and Zhang 2004). It was shown that the model contained compensatory deficiencies: excessive high clouds and deficient middle-top clouds compensated for errors in longwave forcing, while excessive optically thick clouds and deficient optically medium clouds compensated for errors in shortwave forcing (Lin and Zhang 2004). Importantly, the authors noted that the general lack of middle- and low-top optically intermediate and thin clouds was associated with the inability of the model convection to produce clouds (Lin and Zhang 2004).

This work describes the development of a new method for parameterizing the fractional coverage of convective cloud and its implementation within RegCM3–IBIS. It will be shown that the new method allows for simulation of an appropriate convective–radiative feedback that is absent in the default version of RegCM3, improving the convective cloud profile and providing for more physical realism throughout the model.

2. Parameterization methods for convective cloud fraction

a. Commonly used methods in large-scale climate models

It was noted by Arakawa (2004) that there was no need to determine fractional cloud cover for the "classical objectives" of cumulus parameterization, which were to evaluate the vertical distributions of cumulus heating and moistening. Therefore representations of convective cloud fraction in large-scale climate models have often been nonphysical or neglected altogether. In their seminal work describing a convective parameterization scheme based on quasi-equilibrium theory, Arakawa and Schubert (1974) assumed that the fractional area (FC) covered by active cumulus updrafts is negligibly small (i.e., FC $\ll$ 1) and thus provided no calculation of the convective cloud cover. But fractional cloud cover is required for the "non-classical objectives" of cumulus parameterization described by Arakawa (2004), which include the interactions of convection with radiation. Very few formulations for convective cloud fraction have been developed to explicitly simulate this type of cloudiness within large-scale climate models.

In the model described by Sundqvist et al. (1989), convective cloud fraction is a function of the characteristic time scale for convection, cloud depth (number of vertical model layers containing cloud), and grid-scale relative humidity. In this method, fractional cloud cover increases with increasing cloud depth and grid-scale relative humidity. If the top level of a convective cloud has a temperature of $-20°C$ or less, the condensate at that level is treated as stratiform clouds to allow for representation of a convective anvil (Sundqvist et al. 1989).

Tiedtke (1993) considered convective clouds to be condensates produced in cumulus updrafts and detrained into the environmental air. The sources of convective cloud water content and convective cloud cover were described as functions of the detrainment of mass from the convective updraft, specific content of cloud water in the updrafts, and the density of cloudy air. Updraft air was assumed to detrain simultaneously into cloud-free air as well as into already existing clouds, ensuring realistic limits at zero cloud cover (updraft air detrains only into clear air) and at full cloud cover (all updraft air detrains into existing clouds) (Tiedtke 1993). The detrainment mass is obtained from the cumulus parameterization for the updraft mass flux.

In testing, the simulated convective cloud cover using the Tiedtke scheme was shown to reproduce some of the observed global cloud characteristics, such as a cloudy

maximum over the ITCZ and minima over the subsidence regions of Australia, North Africa, southern Africa, and South America. However, significant errors in the amount of fractional cloud cover were noted. High cloud amount was significantly overestimated over the tropics, including the Maritime Continent region, while low and midlevel clouds were underestimated (Tiedtke 1993).

While both the Sundqvist et al. (1989) and Tiedtke (1993) formulations link convective cloud fraction to attributes of the convective motion, neither scheme captures the effects of subgrid variability in convective activity [i.e., variations in updraft mass flux and cloud liquid water (CLW) that are small in scale relative to the size of a model grid cell] on cumulus cloud formation.

Other methods used by global climate models (GCMs) relate convective cloud fraction to some aspect of convective activity, but without recognition of any subgrid variability in condensate or cloud fraction. In the Max Planck Institute's ECHAM5 model (Roeckner et al. 2003), the fractional area occupied by a convective cloud ensemble is a function of the difference in elevation between the detrainment level and top of the cloud. Roeckner et al. (2003) noted that the treatment of convective cloud cover in the ECHAM5 model is arbitrary, stating ''there is no particular reason for choosing this particular function.'' In the Hadley Centre Global Environment Model, version 1 (HadGEM1; Martin et al. 2006), convective cloud fraction is diagnosed from the logarithm of the total water flux and applied as a constant value between cloud base and top. In NCAR's Community Atmosphere Model, version 4 (CAM4; Neale et al. 2010), convective cloud fraction is a linear function of the logarithm of the convective mass flux.

Bony and Emanuel (2001) have provided the only example these authors could find of an attempt to explicitly link subgrid variability in convective cloud water content and cloud fraction to convective activity. Their approach was to consider that the convection parameterization scheme should predict the in-cloud water content, while a statistical cloud scheme should predict how this cloud water is spatially distributed within the domain. Condensed water is produced at the subgrid scale by cumulus convection and at the large scale by supersaturation. This scheme therefore makes no distinction between convective and stratiform clouds, but instead accounts for all types of clouds that may be associated with cumulus convection (Bony and Emanuel 2001).

The total cloud fraction is obtained from integrating the probability density function (PDF) that describes the subgrid variability around the mean total water content q_t. The PDF chosen was of a generalized lognormal form, which requires determination of the first three statistical moments (mean, variance, and skewness

coefficient) of the subgrid-scale fluctuations of the total water mixing ratio (Bony and Emanuel 2001). If there is no subgrid-scale variability within the domain, the parameterization becomes equivalent to an all-or-nothing large-scale saturation scheme (Bony and Emanuel 2001). The authors make the hypothesis that the variance and skewness coefficients of the PDF can be diagnosed (i) from the in-cloud water content predicted by the convection scheme, (ii) from the degree of saturation of the large-scale environment, and (iii) by insisting that the total water mixing ratio values are positive, and solving for these coefficients using the iterative method of Newton (Bony and Emanuel 2001).

While this scheme is certainly more sophisticated than other proposed methods, there are two issues with its practical implementation in a large-scale climate model. First, it has a higher computational expense than other methods because of its dependence on the first three statistical moments of the PDF, the iterative calculation required to determine these moments, and evaluation of the error function that results from the integral. Second, it lumps together all the condensate within a grid cell, but most GCMs and RCMs require a separate resolvable (i.e., nonconvective) cloud fraction for calculation of the resolvable rainfall and for specification of different cloud optical properties for radiative transfer. This scheme is therefore not optimally suited to the structure of current large-scale climate models and, to the best of our knowledge, it has not yet been implemented in any of the more commonly used models.

b. Existing parameterization of convective cloud fraction within RegCM3

The existing horizontal fractional cover of convective cloud (FC_{cnv}) within each grid cell is calculated according to

$$FC_{cnv} = 1 - 0.75^{1/N}, \qquad (1)$$

where N is the number of model layers between cloud top and cloud base, which is determined by the convective parameterization scheme. This function allows for a maximum vertically integrated FC_{cnv} value of 0.25. It is assumed that the cloud fraction in a grid column is distributed randomly in space between the model layers. Within each layer, clouds fill the grid cell uniformly in the vertical direction. The relationship is constant in time and space and is used with all of the convective parameterization schemes available with RegCM3.

This formulation for FC_{cnv} was initially developed for RegCM, version 2 (RegCM2; Giorgi et al. 1993). In that model, some assumptions needed to be made concerning the calculation of FC_{cnv} and CLW, which are input

TABLE 1. Observations of cloud liquid water content used to calculate new convective cloud fraction.

Cumulus cloud type	Liquid water content (g m^{-3})	Location/description	Reference
Continental	0.1–3	Java, Indonesia, influenced by land-derived aerosols	Rosenfeld and Lensky (1998)
	1	Montana, United States	Rogers and Yau (1989)
Maritime	0.25–1.3	Kwajalein Atoll, western Pacific Ocean	Rangno and Hobbs (2005)
	0.4–1.2	Eastern Australian coast, warmer than freezing, 2000–10 000 ft deep	Warner (1955)

variables to the Community Climate Model, version 3 (CCM3), radiative transfer scheme used in RegCM (F. Giorgi 2013, personal communication). The assumption of a maximum vertically integrated FC$_{cnv}$ value of 0.25 was based on the existing structure of CCM3, which also assumed a fixed value of FC$_{cnv}$ (0.3 in that model). Since the CCM3 radiation code also used the random overlap assumption, which tends to maximize the total cloud cover, Eq. (1) was needed to ensure that the total FC$_{cnv}$ did not exceed the prescribed value of 0.25 (F. Giorgi 2013, personal communication).

Additionally, once the total cloud fraction is calculated within the radiation scheme in RegCM3, the scheme does not assume that part of the grid volume is cloud free and part cloudy, but rather adopts an "average cloudiness" based on the total cloud fraction and CLW. In other words, the grid volume is "hazy" instead of being partly sunny and partly cloudy (this assumption has been altered in the latest version of RegCM ; Giorgi et al. 2012). This assumption tends to maximize the absorption of solar radiation and the infrared emission. For these reasons, the maximum vertically integrated FC$_{cnv}$ was reduced (from 0.3 in CCM3 to 0.25 in RegCM3) to avoid excessive cloudiness as seen from the surface (F. Giorgi 2013, personal communication).

The existing formulation in RegCM3 is problematic because it prohibits vertical variability in cloud cover, since each layer within a column experiencing convective motion is required to have the same fractional cloud cover without regard to temporal or spatial variability resulting from rainfall, evaporation, and turbulent mixing. The formulation also results in the unrealistic outcome that stronger convection produces smaller fractional cloud cover per grid cell, since deeper convective motion will result in a larger value of N and consequently smaller FC$_{cnv}$ per layer.

Additionally, RegCM3 assigns a uniform value of the within-cloud CLW that is not physically realistic: 0.3 g m^{-3} for the Grell or Kuo convection schemes and 0.05 g m^{-3} for the Emanuel scheme. These values are considerably less than the observed value of around 1 g m^{-3} (e.g., Rogers and Yau 1989; Emanuel 1994;

Rosenfeld and Lensky 1998), and there is no spatial variability to represent the observed differences between maritime and continental clouds (see Table 1).

The default values of within-cloud convective CLW in RegCM3 were intended to account for the fact that cloud cover is assumed uniform in the vertical direction within a grid volume. Since some model layers can extend to 1 km in depth or greater, but real clouds may be much thinner, assigning a value of within-cloud CLW considerably less than 1 g m^{-3} was intended to represent the average CLW over the depth of a cloudy grid volume (F. Giorgi 2013, personal communication).

However, considerable model testing indicated that the large majority of convective clouds simulated by RegCM3 are in the lower 6 km of the atmosphere, where the model layers are much thinner, while nonconvective clouds dominate in the upper atmosphere where model layers are thicker. In addition, since the model user has control over the number and thickness of model layers, it is possible to assign thin layers representative of actual cloud depth. Hence it is considered that the value of within-cloud CLW prescribed in the model should be close to observed values.

3. New parameterization method for convective cloud fraction

The ideas that form the basis of this work come from Eltahir and Bras (1993), who developed a method to calculate the fractional coverage of rainfall in large-scale climate models based on observations of average rainfall intensity. Eltahir and Bras (1993) compiled rainfall data from a number of convective storms in the tropics, subtropics, and midlatitudes to show that the relationship between rainfall volume and storm area is close to being linear. It was shown that the same relationship can be used to infer the storm area from the rainfall volume simulated by a climate model, if the average rainfall intensity at a given location is known from observations (Eltahir and Bras 1993).

Similarly, a relationship can be derived that uses the CLW simulated by a climate model to infer the

fractional area covered by a convective cloud. When convective cloud forms over some fraction FC of a large area, in this case the grid cell of a large-scale climate model (GCM or RCM, where the size of the grid cell is much larger than the scale of a cumulus cloud), the distribution of CLW over that grid cell can be described statistically by the following mixed distribution:

$$g_{CLW} = FC \times f_{CLW} + (1 - FC) \times \delta(CLW - 0), \quad (2)$$

where g_{CLW} is the PDF of CLW over the total area, FC the fractional area of the grid cell containing cloud, δ the Dirac delta function, and f_{CLW} the conditional PDF of CLW, given that CLW is greater than zero.

At this stage, no assumptions are made about the form of the PDF f_{CLW}, and therefore the description above is

general and always valid. The observed form of f_{CLW} has been fitted to a lognormal distribution (Foster et al. 2006) and to a Weibull distribution (Iassamen et al. 2009), but this current work does not require the PDF to be explicitly specified.

It is assumed here that the mean of f_{CLW} is invariant in time. This assumption seems reasonable given that observations of CLW in convective clouds typically fall within a limited range, as shown in Table 1. The assumption of temporal invariance in the mean of f_{CLW} is an idealization and it is possible that the real mean will vary between cloud systems at the same location. The mean of the conditional PDF f_{CLW} is denoted by CLW_{clim} and may be geographically variable, taking a different value over land and ocean.

The expected value of CLW over a model grid cell is given by

$$E(CLW) = \int_{CLW=0}^{\infty} (CLW \times g_{CLW}) dCLW = (1 - FC) \times 0 + FC \int_{CLW=0+}^{\infty} (CLW \times f_{CLW}) dCLW = CLW_{clim} FC,$$

$$(3)$$

where CLW_{clim} is the mean of the conditional PDF f_{CLW}, which implies that

$$FC = \frac{E(CLW)}{CLW_{clim}}. \quad (4)$$

The $E(CLW)$ can be taken as the simulated grid-average value of CLW, which is a prognostic variable in most large-scale climate models and will hereafter be denoted as $\overline{CLW}$. This leads to an expression for the fractional area of a model grid cell that is covered by convective cloud:

$$FC_{cnv} = \frac{\overline{CLW}}{CLW_{clim}}. \quad (5)$$

The observations in Table 1 suggest that $CLW_{clim} \approx 1.2 \, g \, m^{-3}$ over land and $CLW_{clim} \approx 0.7 \, g \, m^{-3}$ over ocean. It is noted that these values of CLW_{clim} are chosen from within an observed range; there is some flexibility in the choice of these values that could be explored by the model user.

The new formulation has three major advantages over the existing representation of convective cloud cover in RegCM3: 1) The simulated cloud cover is linked explicitly to the simulated CLW and is also tied to physically observed CLW; 2) it recognizes the subgrid variability in CLW that exists in reality and should be accounted for in the model; 3) only one parameter

requires specification to implement this function into RegCM3 (CLW_{clim}), which can be taken from observational data, making it easy to implement consistently across different convection schemes; and 4) the new formulation is independent of grid resolution. The new formulation is therefore more physically realistic than the existing scheme in RegCM3 and it is independent of specific model user decisions. Additionally, the formulation does not add any computational burden to the model.

Both Xu and Randall (1996) and Bony and Emanuel (2001) have noted that local cloud-scale microphysical processes (such as transformations between water species) should be formulated within models in terms of the local concentrations, rather than gridcell averaged concentrations. To the first order, these local concentrations are equal to the gridcell averaged concentrations divided by the cloud amount (Xu and Randall 1996; Bony and Emanuel 2001). The formulation for convective cloud cover presented here is consistent with this reasoning.

4. Simulations using the new parameterization for convective cloud fraction

a. Model description

This work uses the Regional Climate Model, version 3, coupled to Integrated Biosphere Simulator (Winter et al. 2009) as described in Gianotti et al. (2012),

including the subgrid explicit moisture (SUBEX) scheme (Pal et al. 2000) for resolvable, nonconvective clouds and precipitation, the choice of the Grell (Grell 1993) with Fritsch–Chappell (Fritsch and Chappell 1980) or Arakawa–Schubert (Grell et al. 1994) closures, and Emanuel (Emanuel 1991; Emanuel and Živković-Rothman 1999) convective parameterization schemes. Further details of the developments and description of RegCM3 are available in Pal et al. (2007).

Giorgi et al. (2012) describes upgrades that were incorporated into the more recent RegCM, version 4 (RegCM4), which was made publicly available in 2011. RegCM4 does not contain any upgrades to cloud parameterization relevant to this work.

Some modifications were made to the boundary layer parameterization scheme (Holtslag et al. 1990; Holtslag and Boville 1993) within RegCM3, the simulation of large-scale clouds within the PBL, soil thermal conductivity, and the ocean surface roughness (Gianotti 2012). The vertical limit on simulated cloud cover was also extended to permit clouds to form up to an altitude of about 16 km. The combination of these modifications resulted in small reductions to the land and ocean surface latent heat fluxes, a substantial reduction in the PBL height, removing an overestimation bias in the PBL height over land at night, and removal of egregious nighttime low-level large-scale clouds over land (Gianotti 2012). However, none of these modifications significantly impacted the simulation of radiative fluxes or rainfall. Simulations using these modifications are included here for comparison to the default version of the model and are labeled "modified."

b. Experimental design

Simulations were run using both the Grell with Fritsch–Chappell (F-C) closure and Emanuel convection schemes to test the new formulation for FC_{cnv}, using the modified version of RegCM3–IBIS as described above. These simulations are labeled "new." The default function for FC_{cnv} was replaced with the new formulation, using $CLW_{clim} = 1.2 \, g \, m^{-3}$ for land and $CLW_{clim} = 0.7 \, g \, m^{-3}$ for ocean. These values for CLW_{clim} were also used to replace the default values of within-cloud CLW.

One other change was made to the new simulation using the Emanuel scheme: the threshold value at which convective CLW is converted into rainfall. In the default version of the Emanuel scheme, all CLW in excess of a threshold (CLW_T) is converted into rainfall, where the default value of CLW_T is $1.1 \, g \, kg^{-1}$. This represents a cloud water content similar to that observed at the point scale, as shown in Table 1. But in the simulation, this threshold value is compared to a grid-mean value of

TABLE 2. List of parameters used in SUBEX and their default values (based on Pal et al. 2000).

Parameter	Land	Ocean
Cloud formation threshold RH_{min}	0.8	0.9
Maximum saturation RH_{max}	1.01	1.01
Autoconversion rate C_{ppt} (s^{-1})	5×10^{-4}	5×10^{-4}
Autoconversion scale factor C_{acs}	0.65	0.3
Accretion rate C_{acc} $(m^3 \, kg^{-1} \, s^{-1})$	6	6
Raindrop evaporation rate C_{evap} $[(kg \, m^{-2} \, s^{-1})^{-1/2} \, s^{-1}]$	2×10^{-5}	2×10^{-5}

simulated CLW. Thus the appropriate comparison needs to be a grid-mean value of CLW_T, and so the value of CLW_T was reduced to $0.25 \, g \, kg^{-1}$. We note here that choosing model parameters in this way is not ideal, and that a more robust method for simulating the conversion of convective cloud water into rainfall is needed. This issue is addressed and resolved in Gianotti and Eltahir (2014, hereafter Part II).

Table 2 presents the parameter values used in the SUBEX routine in this study. The default values were obtained from the original version of the model, as described in Pal et al. (2000). It should be noted that, although the large-scale SUBEX routine and the convective parameterization schemes operate independently within the RegCM3 structure, each routine can significantly impact the other by altering grid-scale variables such as temperature and water vapor. Therefore the model user should be cognizant of how changes introduced to the large-scale scheme affect convection and vice versa. Different results using the new FC_{cnv} parameterization presented here will be obtained if changes are made to the SUBEX routine.

The model domain (Fig. 1) was centered along the equator at 115°E, used a normal Mercator projection, and spanned 95 grid points meridionally and 200 grid points zonally, with a horizontal resolution of 30 km. The simulations used 18 vertical sigma levels, from the ground surface up to the 50-mb level. In all simulations presented, the land surface scheme was run every 120 s, twice the model time step.

Sea surface temperatures (SSTs) were prescribed using the National Ocean and Atmospheric Administration (NOAA) optimally interpolated SST (OISST) dataset, which is available at 1° × 1° resolution and at a weekly time scale (Reynolds et al. 2002). Topographic information was taken from the United States Geological Survey's Global 30-arc-s elevation dataset (GTOPO30), aggregated to 10 arc min (United States Geological Survey 1996). Vegetation biomes were based on the potential global vegetation dataset of Ramankutty (1999), modified to include two extra biomes for inland
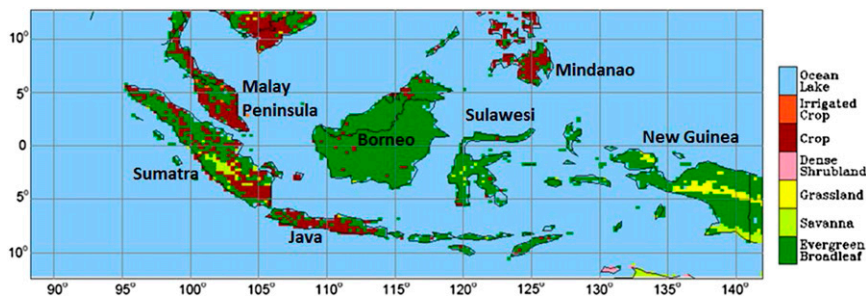
FIG. 1. Model domain showing vegetation classification used for IBIS. The domain has been sized such that it covers the generally accepted extent of the Maritime Continent region. Major islands are labeled.

water and ocean as described in Winter et al. (2009). In all simulations presented, RegCM3–IBIS was run only with static vegetation.

Soil properties, such as albedo and porosity, were determined based on the relative proportions of clay and sand in each grid cell. Sand and clay percentages were taken from the Global Soil Dataset (Global Soil Data Task, IGDP-DIS 2000), which has a spatial resolution of 5 min. Soil moisture, temperature, and ice content were initialized using the output from a global $0.5° \times 0.5°$ resolution 20-yr offline simulation of IBIS as described in Winter et al. (2009).

The 40-yr European Centre for Medium-Range Weather Forecasts (ECMWF) Re-Analysis (ERA-40) dataset (Uppala et al. 2005), available from September 1957 to August 2002, was used to force the boundaries. The exponential relaxation technique of Davies and Turner (1977) was used with both datasets.

Simulations began on 1 July 1997 and ended 31 December 2001. The first 6 months of output were ignored to allow for spinup. The resulting four years of simulation (1998–2001) were used for evaluation of model performance. This time period was chosen for maximal overlap between the dataset used for lateral boundary conditions and the Tropical Rainfall Measuring Mission (TRMM) rainfall observational dataset used for comparison (described below). Six simulations are presented in this study. Table 3 summarizes the different characteristics of these simulations and lists the names used to reference each simulation throughout the text.

c. Comparison datasets

Several datasets are used for comparison to model output in this study.

Solar radiation is compared to the National Aeronautics and Space Administration (NASA)/Global Energy and Water Cycle Experiment (GEWEX) Surface Radiation Budget (SRB) dataset release 3.0 (Stackhouse et al. 2011), obtained from the NASA Langley Research Center Atmospheric Sciences Data

Center. This dataset is available at 3-hourly intervals on a $1° \times 1°$ global grid. The data were interpolated to the model domain for direct comparison to simulation output.

Observations of latent heat flux over land are taken from direct observations of evapotranspiration (ET) in the Maritime Continent region, as described in Table 4 of Gianotti et al. (2012). Over ocean, latent and sensible heat flux observations are from the Woods Hole Oceanographic Institution (WHOI) global dataset of ocean evaporation (Yu et al. 2008). The WHOI observations compare well with data collected during the Tropical Ocean and Global Atmosphere Coupled Ocean–Atmosphere Response Experiment (TOGA COARE) (Webster et al. 1996; Weller and Anderson 1996; Lau and Sui 1997; Sui et al. 1997; Emanuel and Živković-Rothman 1999).

Total rainfall is compared to data from the TRMM Multisatellite Precipitation Analysis (TMPA) $0.25° \times 0.25°$ resolution 3B42 product (described in Huffman et al. 2007), referenced in this work simply as TRMM. TRMM is available from January 1998 to the present day, and is one of the highest resolution datasets available over the Maritime Continent. Relative proportions of convective and large-scale rain are taken from Mori et al. (2004), who used the 2A25, 2A12, and 2B31

TABLE 3. Varying characteristics of simulations used in study. The names are used to reference each simulation in the text.

Simulation name	Convection scheme	PBL region*	Convective cloud fraction
GFC-Def	Grell with F-C	Default	Default
GFC-Mod	Grell with F-C	Modified**	Default
GFC-New	Grell with F-C	Modified**	New
EMAN-Def	Emanuel	Default	Default
EMAN-Mod	Emanuel	Modified**	Default
EMAN-New	Emanuel	Modified**	New

* Refers to simulation of PBL height, ocean surface roughness, soil heat flux, and large-scale clouds within the PBL region.
** As described in Gianotti (2012).

TRMM products to describe the climatological convective versus stratiform rainfall split over Indonesia.

5. Results and discussion

a. Cloud fraction

Figures 2 and 3 present the simulated mean diurnal cycle of the vertical structure of cloud cover over 1998–2001 for land grid cells within the domain. Note that these figures present the total cloud cover, which is a combination of convective (primarily located in the lower atmosphere during the daytime) and large-scale (primarily located in the upper atmosphere at all times and lower atmosphere at night) components. The figures compare the default, modified, and new simulations for both the Grell with Fritsch–Chappell and Emanuel convection schemes. Only the land-based cloud fraction is shown as cloud fraction over ocean does not exhibit a significant diurnal cycle.

The results show that the default and modified simulations with both convection schemes lack an appropriate representation of low and middle cloud cover associated with daytime convection. Specifically, cloud cover in the lower atmosphere is actually at a minimum when convective activity is strongest, in the early afternoon. This region of the atmosphere would be expected to contain some convective cloud cover during this time of day. The lack of cloud cover here is as a result of the default convective cloud cover formulation in RegCM3. Cloud depth with the Emanuel scheme can be quite large—up to 10 layers—resulting in a cloud fraction of only 3% per model layer during the afternoon when convection is at its strongest. Even with the Grell scheme, a cloud depth of five layers is commonly simulated, resulting in a cloud fraction of around 5%.

The GFC-Def simulation (see Table 3 for simulation names and characteristics) produces some low cloud cover in the afternoon, concomitant with convective activity, but model testing showed that this was almost entirely erroneous large-scale cloud cover produced by the SUBEX routine inside the mixed PBL. Since convective mass flux is relatively weak with the Grell scheme, some moisture builds up in the lower atmosphere during the day as a result of turbulent surface fluxes, which the SUBEX routine converts into cloud cover. This low cloud cover is largely removed in GFC-Mod because of a new representation of large-scale cloud cover that requires bulk saturation within the mixed PBL (Gianotti 2012).

These results therefore illustrate the nonphysical outcome that results from the default version of convective cloud fraction in RegCM3. Convection, although responsible for producing rainfall and transporting moisture aloft to form large-scale clouds, does not play a significant role in the formation of low and midlevel cloud cover.

By contrast, Figs. 2 and 3 show that both GFC-New and EMAN-New exhibit a distinct diurnal cycle in cloud cover at low and middle levels over land. The presence of convective motion is clearly visible, with cloud present in the 0930–1530 local time (LT) window approximately 2–8 km above the surface. This cloud is in the precise location that we would expect to see cumulus clouds resulting from daytime convection, indicating that the new formulation is working as intended.

Figures 2 and 3 highlight that the Emanuel scheme produces much more CLW, as the result of a stronger convective mass flux, than the Grell scheme. This was to be expected given the significant volume of rainfall simulated by the Emanuel scheme compared to the Grell scheme [e.g., as shown in Gianotti et al. (2012)]. Hence when the simulated CLW is used to calculate the convective cloud cover, the Emanuel scheme produces a greater fractional cloud area than the Grell scheme.

It is noted that the low-level cloud cover in GFC-New is comparable in magnitude to that in GFC-Def, which might lead one to question the utility of the new parameterization. However, these similarities are coincidental since the cloud cover in GFC-Def was from the large-scale SUBEX routine and was not related to the active convective motion. Therefore it is considered that the cloud cover in GFC-New represents an improvement in physical realism, if not in the actual cloud cover.

The simulations with the Emanuel scheme exhibit a distinct diurnal cycle in high cloud cover, with more cloud generated in the late afternoon and nighttime, while the Grell simulations do not exhibit the same degree of diurnal variability. This again is the result of relative differences in convective mass flux between these schemes. Convective updrafts transport moisture into the upper atmosphere, where it detrains and is then added to the large-scale water vapor content. The increase in humidity is converted by the SUBEX routine into large-scale cloud cover. Daytime convection is much weaker with the Grell scheme and less moisture is transported aloft than with the Emanuel scheme, resulting in less high cloud cover. The simulation of high large-scale clouds at night is consistent with observations over the Maritime Continent, in which convective anvils and mesoscale convective systems (which can be thought of as a hybrid of convective and nonconvective rainfall) persist throughout the night over the islands (e.g., Ichikawa and Yasunari 2006, 2008).

A comparison between the simulated cloud fraction and observations from the International Satellite Cloud Climatology Project (ISCCP) is provided in Part II of this paper series.
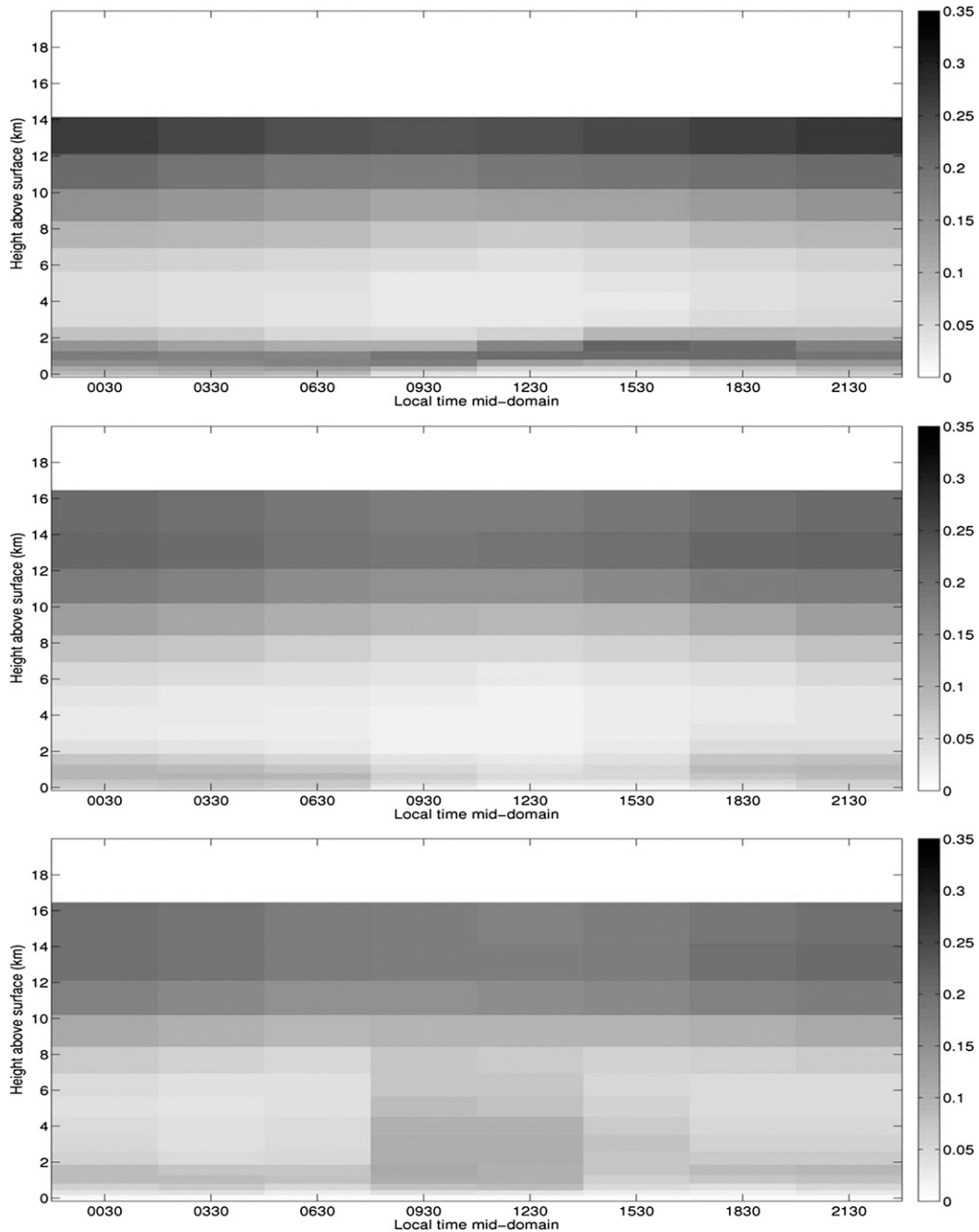
FIG. 2. Diurnal cycle of cloud cover averaged over land grid cells within the model domain over period 1998–2001 for simulations (top) GFC-Def, (middle) GFC-Mod, and (bottom) GFC-New. Note that these figures present the total cloud cover, which is a combination of convective (primarily located in the lower atmosphere during the daytime) and large-scale (primarily located in the upper atmosphere at all times and lower atmosphere at night) components. The x-axis labels indicate the time at the middle of each 3-h output window, with respect to local time in the center of the model domain. To represent the y axis on a linear scale, the vertical extent of each model layer was assigned a single value of cloud cover, as provided by the model output. In reality, a smoother profile with less abrupt vertical variability would be expected.

b. Radiative and turbulent heat fluxes

Figures 4 and 5 show the average diurnal cycle of incoming solar radiation (insolation) received at the surface over land and ocean with both the Grell and Emanuel schemes, comparing the new simulations to the modified simulations and the SRB observations. Mean daily values are given in parentheses. The default simulations are not
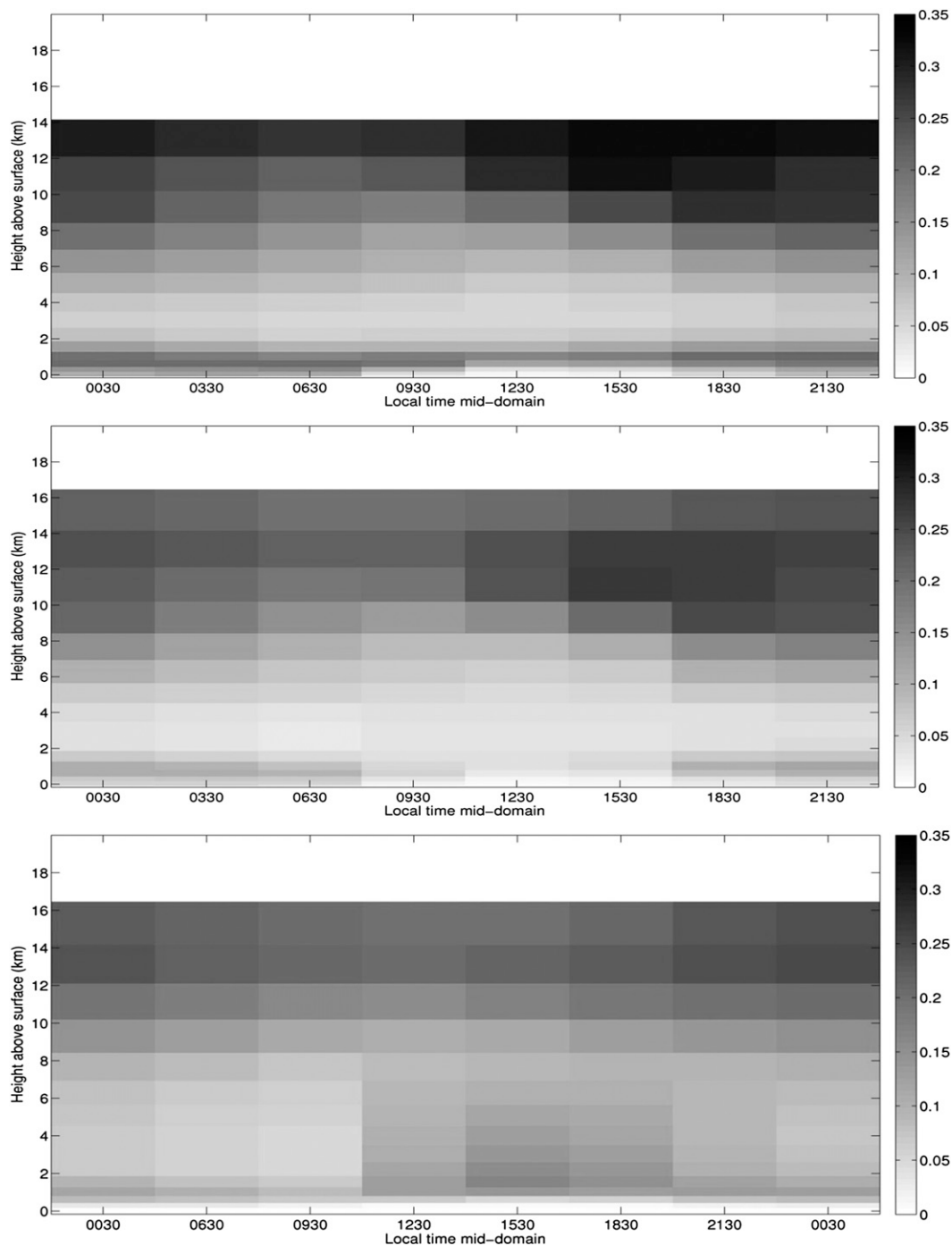
FIG. 3. As in Fig. 2, but for simulations (top) EMAN-Def, (middle) EMAN-Mod, and (bottom) EMAN-New.

shown to avoid overcluttering the figures, but the shapes of the diurnal cycles of insolation were very similar to the modified simulations.

With both GFC-Mod and EMAN-Mod, the default convective cloud fraction results in significant over-estimation of insolation over both land and ocean during the early and midafternoon, with the peak insolation overestimated by 150–200 W m^{-2}. The simulated peak insolation occurs in the early afternoon, in contrast to the observed late morning peak shown in the SRB data. These results are consistent with the lack of cloud cover produced by GFC-Mod and EMAN-Mod while daytime
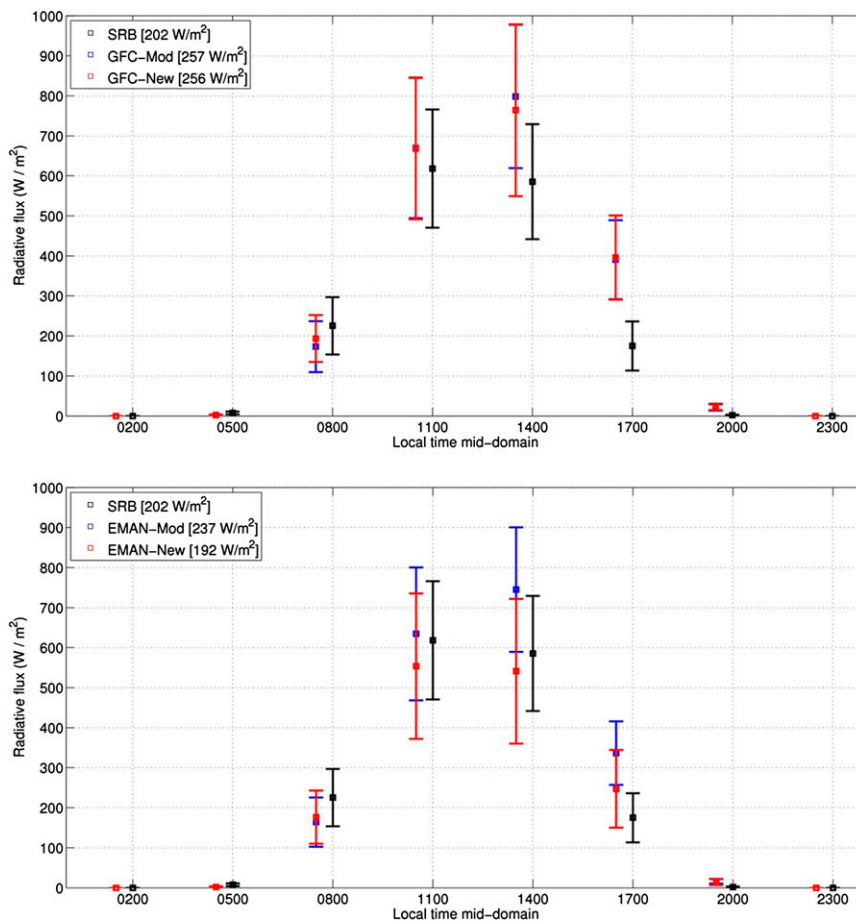
FIG. 4. Diurnal cycle of incoming solar radiation averaged over land for period 1998–2001 for SRB observations and simulations using (top) Grell with Fritsch–Chappell and (bottom) Emanuel convection schemes. Square symbols indicates the mean value; error bars indicate ±1 standard deviation.

convection is active. This indicates that the default convective cloud fraction in RegCM3 does not allow for representation of a convective–radiative feedback.

With GFC-New, insolation changed negligibly over land and increased slightly over ocean compared to GFC-Mod, perpetuating a significant overestimation in insolation during the early and midafternoon. These results reflect the relatively small change to the vertically integrated cloud cover between these simulations. Hence these results suggest that the Grell scheme does not produce sufficient convective cloud liquid water to significantly influence the insolation at the surface.

In contrast, insolation during the afternoon substantially decreased from EMAN-Mod to EMAN-New over both land and ocean because of the increase in convective cloud cover with this scheme, producing a small underestimation over land and a large underestimation over ocean. The results indicate that the new convective cloud fraction allows for simulation of a convective–radiative feedback. The strength of the feedback is overestimated, with too much cloud cover and consequently too little insolation reaching the surface during the afternoon. However, the timing and direction of the feedback is physically realistic and therefore considered to be an improvement upon the previous version of the model.

Changes to the surface net radiation and turbulent fluxes are summarized in Table 4. These results are consistent with the simulated cloud cover and illustrate the mixed performance of the two convection schemes, with some model results showing improvement and others deteriorating compared to observations.

Over land, both net shortwave radiation and net surface radiation are overestimated in all three of the GFC simulations, with worse bias in GFC-Mod and GFC-New than in GFC-Def. In contrast, net shortwave radiation and net surface radiation are overestimated in both EMAN-Def and EMAN-Mod but underestimated
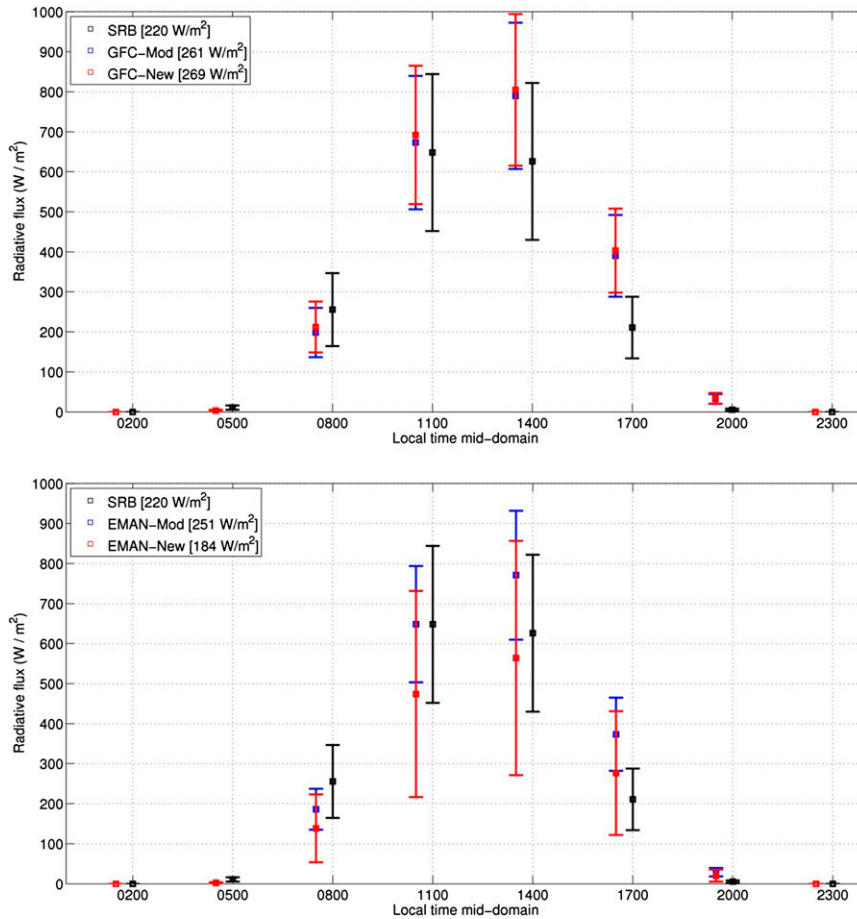
FIG. 5. As in Fig. 4, but for diurnal cycle of incoming solar radiation averaged over ocean.

in EMAN-New. The bias in net shortwave radiation is minimized in EMAN-New, while the bias in net surface radiation is equivalent in EMAN-Def (overestimated) and EMAN-New (underestimated).

Over ocean, net shortwave radiation and net surface radiation did not change significantly (less than 4% difference) between the three GFC simulations, reflecting the minimal differences in ocean-based cloud cover between these simulations. All three GFC simulations show significant overestimation of net shortwave and net surface radiation over the ocean compared to observations. By contrast, the new convective cloud fraction led to a significant decrease in net shortwave and net surface radiation in EMAN-New, corresponding to significant changes in ocean-based cloud cover. The underestimation bias in EMAN-New is roughly the same as the overestimation bias in EMAN-Def and EMAN-Mod.

Planetary albedo decreased progressively from GFC-Def to GFC-Mod and then GFC-New, resulting in underestimation compared to the observed albedo. In contrast, reductions in planetary albedo between EMAN-Def, EMAN-Mod, and EMAN-New improved the model results, with a good match in albedo between EMAN-New and observations.

All simulations presented here exhibit reasonable representation of longwave radiation; mean daily values of longwave radiation both down to the surface and up from the surface are within $15\,\mathrm{W\,m^{-2}}$ (i.e., 4% bias) of observations over land and ocean.

Over land, the sensible heat flux (SH) and latent heat flux (LH) changed only slightly with GFC-New compared to GFC-Mod, reflecting the minor changes to radiative fluxes. Both LH and SH exhibit overestimation biases compared to observations in all of the GFC simulations. LH decreased significantly in EMAN-New compared to EMAN-Def and EMAN-Mod, reflecting the change to the diurnal cycle of insolation and net radiation at the surface. This decrease brought the simulated LH in EMAN-New much closer to observations. SH still exhibits some underestimation bias in EMAN-New compared to observations, but the bias is

TABLE 4. Average daily surface radiation and turbulent heat fluxes over period 1998–2001 for (top) land and (bottom) ocean cells within the domain. All radiative and turbulent fluxes are in units of $W\,m^{-2}$.

Product/simulation	SW_{dn}	SW_{up}	SW_{net}	Land albedo	Planetary albedo	LW_{dn}	LW_{up}	R_N	LH	SH
					Land					
Observations	202	31	171	16%	48%	411	452	129	95	34
GFC-Def	225	31	194	14%	45%	411	464	141	104	36
GFC-Mod	257	35	222	13%	44%	401	459	164	118	48
GFC-New	256	35	221	13%	41%	396	457	160	112	50
EMAN-Def	213	30	183	14%	50%	416	457	141	134	6
EMAN-Mod	237	33	204	14%	49%	409	456	157	137	21
EMAN-New	192	27	165	14%	48%	410	455	117	100	18
					Ocean					
Observations	220	14	206	6%	45%	420	467	158	108	10
GFC-Def	264	17	247	6%	40%	414	473	188	129	12
GFC-Mod	261	16	245	6%	43%	413	473	184	128	15
GFC-New	269	17	252	6%	40%	408	473	187	129	17
EMAN-Def	257	16	241	6%	45%	418	473	186	126	4
EMAN-Mod	251	16	235	6%	49%	420	473	182	118	7
EMAN-New	184	12	172	6%	51%	429	473	129	117	5

significantly reduced compared to EMAN-Def. Over ocean, both simulations show only a small change to SH and LH, which is to be expected since the SST is fixed in these simulations.

Therefore it is acknowledged that the surface energy budget with the new simulations does not show consistent improvement across convection schemes. However, the new simulations contain more physically realistic connections between convective motion, cloud cover, and insolation. Therefore it is considered that good model performance that occurred with the default version of the model may have been coincidental or the result of good "tuning." Additionally, the changes made to the model might have positive impacts in ways that are not captured here, for example in simulations over other regions or when looking at other climatic features.

c. Rainfall

Average total, convective, and large-scale rainfall volumes over the period 1998–2001 are shown in Table 5. Again, the results indicate a mixed performance between the two convection schemes.

Simulation with the Grell scheme does not show significant improvements to model performance. Both convective and large-scale rainfall volumes over land increase from GFC-Def to GFC-New, resulting in continued overestimation of the large-scale rainfall and an overestimation in the total rainfall. However, it is noted that the underestimation bias in convective rainfall is slightly reduced in GFC-New. Over ocean, convective rainfall increased from GFC-Def to GFC-New while large-scale rainfall decreased, producing comparable total rainfall but errors in each of the rainfall components. Therefore it does not appear that the new convective cloud fraction had a positive impact on the simulation of rainfall with the Grell scheme. Part II will provide a more detailed discussion of rainfall production using the Grell scheme, including the reasons why improved performance is not shown here.

With the Emanuel scheme over land, total and convective rainfall volumes improved dramatically from EMAN-Def to EMAN-New. While large-scale rainfall over land is overestimated in EMAN-New, this is largely as a result of an overestimation of high large-scale cloud

TABLE 5. Average daily rainfall over land and ocean over period 1998–2001 for each simulation presented in this study, with TRMM values shown for comparison. All values are in units of $mm\,day^{-1}$.

Product/simulation	Land average			Ocean average		
	Total	Convective	Large-scale	Total	Convective	Large-scale
TRMM	8.6	5.4 (63%)	3.2 (37%)	7.0	4.0 (57%)	3.0 (43%)
GFC-Def	8.5	3.7 (43%)	4.8 (57%)	6.7	3.8 (56%)	2.9 (44%)
GFC-Mod	10.9	4.4 (40%)	6.5 (60%)	8.5	4.1 (48%)	4.4 (52%)
GFC-New	9.2	4.1 (45%)	5.1 (55%)	7.3	5.5 (75%)	1.8 (25%)
EMAN-Def	14.9	11.9 (80%)	3.0 (20%)	7.2	6.2 (86%)	1.0 (14%)
EMAN-Mod	16.8	9.9 (59%)	6.9 (41%)	6.7	3.8 (57%)	2.9 (43%)
EMAN-New	10.3	5.0 (49%)	5.3 (51%)	7.9	3.5 (44%)	4.4 (56%)

cover (which is subsequently converted into large-scale rainfall by the SUBEX routine). Over ocean, both convective and large-scale rainfall volumes improved significantly from EMAN-Def to EMAN-New. Again, there is some overestimation of large-scale rainfall in EMAN-New resulting from an overestimation of high large-scale cloud cover, which results in some overestimation of the total rainfall over ocean.

In general it is considered that the new cloud fraction results in significant improvement in rainfall performance using the Emanuel scheme. This illustrates the tight coupling that exists between convection, cloud formation, radiative flux, and rainfall production, and shows how improving the physical realism in the convective–radiative feedback has positive effects on other aspects of the simulation. Further improvements in rainfall performance using the Emanuel scheme will be shown in Part II.

6. Summary

This paper describes a new method for parameterizing convective cloud fraction that can be used within regional and global climate models, and evaluates the new method using the coupled regional-scale model RegCM3–IBIS. The horizontal extent of convective cloud cover is calculated by utilizing a relationship between the simulated amount of convective cloud water and typical observations of convective cloud water density. This formulation not only provides a physically meaningful basis for the simulation of convective cloud cover, but it is also spatially and temporally variable and independent of model resolution, rendering it generally applicable for large-scale climate models.

This work demonstrates that explicitly linking convective cloud fraction to the simulated amount of convective cloud liquid water can significantly impact model performance. The new parameterization for convective cloud fraction presented here produces a diurnal cycle of cloud cover over land that is consistent with convective activity, including simulated cloud in the location and timeframe that is expected as a result of daytime convection.

Simulations over the Maritime Continent show that the new method allows for simulation of an essential convective–radiative feedback that was absent in the existing version of RegCM3–IBIS, such that moist convection not only responds to diurnal variability at the earth's surface but also impacts the solar radiation received at the surface via cumulus cloud production. This result is especially evident when using the Emanuel convection scheme. While the impact of this change on model performance was mixed, this work emphasizes

the importance of explicitly linking convective motion to radiative transfer via cloud cover, consistent with Arakawa's (2004) "new objectives" for convective parameterizations.

Part II will build on this work by presenting a new parameterization for the autoconversion of convective rainfall that explicitly accounts for subgrid variability in cloud water density, and continues the discussion on diurnally varying convective processes.

REFERENCES

Arakawa, A., 2004: The cumulus parameterization problem: Past, present, and future. *J. Climate,* **17,** 2493–2525.

——, and W. H. Schubert, 1974: Interaction of a cumulus cloud ensemble with the large-scale environment, Part I. *J. Atmos. Sci.,* **31,** 674–701.

Bergman, J. W., and M. L. Salby, 1996: Diurnal variations of cloud cover and their relationship to climatological conditions. *J. Climate,* **9,** 2802–2820.

Bony, S., and K. A. Emanuel, 2001: A parameterization of the cloudiness associated with cumulus convection: Evaluation using TOGA COARE data. *J. Atmos. Sci.,* **58,** 3158–3183.

Chow, K. C., J. C. L. Chan, J. S. Pal, and F. Giorgi, 2006: Convection suppression criteria applied to the MIT cumulus parameterization scheme for simulating the Asian summer monsoon. *Geophys. Res. Lett.,* **33,** L24709, doi:10.1029/2006GL028026.

Christensen, J. H., and Coauthors, 2007: Regional climate projections. *Climate Change 2007: The Physical Science Basis,* S. Solomon et al., Eds., Cambridge University Press, 847–940.

Dai, A., and K. E. Trenberth, 2004: The diurnal cycle and its depiction in the Community Climate System Model. *J. Climate,* **17,** 930–951.

Davies, H., and R. Turner, 1977: Updating prediction models by dynamical relaxation: An examination of the technique. *Quart. J. Roy. Meteor. Soc.,* **103,** 225–245.

Eltahir, E. A. B., and R. L. Bras, 1993: Estimation of the fractional coverage of rainfall in climate models. *J. Climate,* **6,** 639–644.

Emanuel, K. A., 1991: A scheme for representing cumulus convection in large-scale models. *J. Atmos. Sci.,* **48,** 2313–2335.

——, 1994: *Atmospheric Convection.* Oxford University Press, 580 pp.

——, and M. Živković-Rothman, 1999: Development and evaluation of a convection scheme for use in climate models. *J. Atmos. Sci.,* **56,** 1766–1782.

Foster, J., M. Bevis, and W. Raymond, 2006: Precipitable water and the lognormal distribution. *J. Geophys. Res.,* **111,** D15102, doi:10.1029/2005JD006731.

Francisco, R. V., J. Argete, F. Giorgi, J. Pal, X. Bi, and W. J. Gutowski, 2006: Regional model simulation of summer rainfall over the Philippines: Effect of choice of driving fields and ocean flux schemes. *Theor. Appl. Climatol.,* **86,** 215–227.

Fritsch, J. M., and C. F. Chappell, 1980: Numerical prediction of convectively driven mesoscale pressure systems. Part I: Convective parameterization. *J. Atmos. Sci.,* **37,** 1722–1733.

Gianotti, R. L., 2012: Convective cloud and rainfall processes over the Maritime Continent: Simulation and analysis of the diurnal cycle. Ph.D. dissertation, Massachusetts Institute of Technology, 306 pp.

——, and E. A. B. Eltahir, 2014: Regional climate modeling over the Maritime Continent. Part II: New parameterization for autoconversion of convective rainfall. *J. Climate,* **27,** 1504–1523.

——, D. Zhang, and E. A. B. Eltahir, 2012: Assessment of the Regional Climate Model version 3 over the Maritime Continent using different cumulus parameterization and land surface schemes. *J. Climate,* **25,** 638–656.

Giorgi, F., M. R. Marinucci, and G. T. Bates, 1993: Development of a second-generation regional climate model (RegCM2). Part II: Convective processes and assimilation of lateral boundary conditions. *Mon. Wea. Rev.,* **121,** 2814–2832.

——, and Coauthors, 2012: RegCM4: Model description and preliminary tests over multiple CORDEX domains. *Climate Res.,* **52,** 7–29.

Global Soil Data Task, IGDP-DIS, 2000: *Global Soil Data Products.* International Geosphere-Biosphere Programme, Data and Information System (IGDP-DIS), CD-ROM. [Available online at http://daac.ornl.gov/SOILS/igbp.html.]

Grell, G. A., 1993: Prognostic evaluation of assumptions used by cumulus parameterizations. *Mon. Wea. Rev.,* **121,** 764–787.

——, J. Dudhia, and D. R. Stauffer, 1994: Description of the fifth-generation Penn State/NCAR Mesoscale Model (MM5). NCAR Tech. Rep. NCAR/TN-398+STR, 117 pp.

Holtslag, A. A. M., and B. A. Boville, 1993: Local versus nonlocal boundary-layer diffusion in a global climate model. *J. Climate,* **6,** 1825–1842.

——, E. I. F. de Bruijn, and H.-L. Pan, 1990: A high-resolution air mass transformation model for short-range weather forecasting. *Mon. Wea. Rev.,* **118,** 1561–1575.

Huffman, G. J., and Coauthors, 2007: The TRMM Multisatellite Precipitation Analysis (TMPA): Quasi-global, multiyear, combined-sensor precipitation estimates at fine scales. *J. Hydrometeor.,* **8,** 38–55.

Iassamen, A., H. Sauvageot, N. Jeannin, and S. Ameur, 2009: Distribution of tropospheric water vapor in clear and cloudy conditions from microwave radiometric profiling. *J. Appl. Meteor. Climatol.,* **48,** 600–615.

Ichikawa, H., and T. Yasunari, 2006: Time-space characteristics of diurnal rainfall over Borneo and surrounding oceans as observed by TRMM-PR. *J. Climate,* **19,** 1238–1260.

——, and ——, 2008: Intraseasonal variability in diurnal rainfall over New Guinea and the surrounding oceans during austral summer. *J. Climate,* **21,** 2852–2868.

Kothe, S., and B. Ahrens, 2010: On the radiation budget in regional climate simulations for West Africa. *J. Geophys. Res.,* **115,** D23120, doi:10.1029/2010JD014331.

Lau, K.-M., and C.-H. Sui, 1997: Mechanisms of short-term sea surface temperature regulation: Observations during TOGA COARE. *J. Climate,* **10,** 465–472.

Lin, W. Y., and M. H. Zhang, 2004: Evaluation of clouds and their radiative effects simulated by the NCAR Community Atmospheric Model against satellite observations. *J. Climate,* **17,** 3302–3318.

Martin, G. M., M. A. Ringer, V. D. Pope, A. Jones, C. Dearden, and T. J. Hinton, 2006: The physical properties of the atmosphere in the new Hadley Centre Global Environmental Model (HadGEM1). Part I: Model description and global climatology. *J. Climate,* **19,** 1274–1301.

Mori, S., and Coauthors, 2004: Diurnal land–sea rainfall peak migration over Sumatera Island, Indonesian Maritime Continent, observed by TRMM satellite and intensive rawinsonde soundings. *Mon. Wea. Rev.,* **132,** 2021–2039.

Neale, R. B., and J. Slingo, 2003: The Maritime Continent and its role in the global climate: A GCM study. *J. Climate,* **16,** 834–848.

——, and Coauthors, 2010: Description of the NCAR Community Atmosphere Model (CAM 4.0). NCAR Tech. Note NCAR/TN-485+STR, 212 pp.

Pal, J. S., E. E. Small, and E. A. B. Eltahir, 2000: Simulation of regional-scale water and energy budgets: Representation of subgrid cloud and precipitation processes within RegCM. *J. Geophys. Res.,* **105** (D24), 29 579–29 594.

——, and Coauthors, 2007: Regional climate modeling for the developing world: The ICTP RegCM3 and RegCNET. *Bull. Amer. Meteor. Soc.,* **88,** 1395–1409.

Ramankutty, N., 1999: Estimating historical changes in land cover: North American croplands from 1850 to 1992. *Global Ecol. Biogeogr.,* **8,** 381–396.

Rangno, A. L., and P. V. Hobbs, 2005: Microstructures and precipitation development in cumulus and small cumulonimbus clouds over the warm pool of the tropical Pacific Ocean. *Quart. J. Roy. Meteor. Soc.,* **131,** 639–673.

Reynolds, R. W., N. Rayner, T. Smith, D. Stokes, and W. Wang, 2002: An improved in situ and satellite SST analysis for climate. *J. Climate,* **15,** 1609–1625.

Roeckner, E., and Coauthors, 2003: The atmospheric general circulation model ECHAM5 Part 1: Model description. Max-Planck-Institut für Meteorologie Rep. 349, 140 pp.

Rogers, R. R., and M. K. Yau, 1989: *A Short Course in Cloud Physics.* Elsevier, 293 pp.

Rosenfeld, D., and I. M. Lensky, 1998: Satellite-based insights into precipitation formation processes in continental and maritime convective clouds. *Bull. Amer. Meteor. Soc.,* **79,** 2457–2476.

Stackhouse, P. W., Jr., S. K. Gupta, S. J. Cox, J. C. Mikovitz, T. Zhang, and L. M. Hinkelman, 2011: 24.5-Year SRB data set released. *GEWEX News,* No. 21, International GEWEX Project Office, Silver Spring, MD, 10–12.

Sui, C.-H., X. Li, K.-M. Lau, and D. Adamec, 1997: Multiscale air–sea interactions during TOGA COARE. *Mon. Wea. Rev.,* **125,** 448–462.

Sundqvist, H., E. Berge, and J. E. Kristjánsson, 1989: Condensation and cloud parameterization studies with a mesoscale numerical weather prediction model. *Mon. Wea. Rev.,* **117,** 1641–1657.

Tiedtke, M., 1988: Parameterization of cumulus convection in large-scale models. *Physically-Based Modelling and Simulation of Climate and Climatic Change,* M. E. Schlesinger, Ed., D. Reidel, 375–431.

——, 1993: Representation of clouds in large-scale models. *Mon. Wea. Rev.,* **121,** 3040–3061.

United States Geological Survey, cited 1996: Global 30-arc second elevation dataset (GTOPO30). [Available online online at http://eros.usgs.gov/#/Find_Data/Products_and_Data_Available/gtopo30_info.]

Uppala, S. M., and Coauthors, 2005: The ERA-40 Re-Analysis. *Quart. J. Roy. Meteor. Soc.,* **131,** 2961–3012. [Dataset available online at http://www.ecmwf.int/research/era/do/get/era-40.]

Wang, Y., L. Zhou, and K. Hamilton, 2007: Effect of convective entrainment/detrainment on the simulation of the tropical precipitation diurnal cycle. *Mon. Wea. Rev.,* **135,** 567–585.

Warner, J., 1955: The water content of cumuliform cloud. *Tellus,* **7,** 449–457.

Webster, P. J., C. A. Clayson, and J. A. Curry, 1996: Clouds, radiation, and the diurnal cycle of sea surface temperature in the tropical western Pacific. *J. Climate,* **9,** 1712–1730.

Weller, R. A., and S. P. Anderson, 1996: Surface meteorology and air–sea fluxes in the western equatorial Pacific warm pool during the TOGA coupled ocean–atmosphere response experiment. *J. Climate,* **9,** 1959–1990.

Winter, J. M., J. S. Pal, and E. A. B. Eltahir, 2009: Coupling of Integrated Biosphere Simulator to Regional Climate Model version 3. *J. Climate,* **22,** 2743–2757.

Xu, K.-M., and D. A. Randall, 1996: A semiempirical cloudiness parameterization for use in climate models. *J. Atmos. Sci.,* **53,** 3084–3102.

Yang, G.-Y., and J. Slingo, 2001: The diurnal cycle in the tropics. *Mon. Wea. Rev.,* **129,** 784–801.

Yu, L., X. Jin, and R. A. Weller, 2008: Multidecade global flux datasets from the objectively analyzed air–sea fluxes (OAFlux) project: Latent and sensible heat fluxes, ocean evaporation, and related surface meteorological variables. Woods Hole Oceanographic Institution OAFlux Project Tech. Rep. OA-2008-01, 64 pp. [Available online at http://oaflux.whoi.edu/pdfs/OAFlux_TechReport_3rd_release.pdf.]